CO_2-fixing one-carbon metabolism in a cellulose-degrading bacterium *Clostridium thermocellum*

Wei Xiong[a], Paul P. Lin[b], Lauren Magnusson[a], Lisa Warner[c], James C. Liao[b,d], Pin-Ching Maness[a,1], and Katherine J. Chou[a,1]

[a]Biosciences Center, National Renewable Energy Laboratory, Golden, CO 80401; [b]Department of Chemical and Biomolecular Engineering, University of California, Los Angeles, CA 90095; [c]National Bioenergy Center, National Renewable Energy Laboratory, Golden, CO 80401; and [d]Academia Sinica, Taipei City, Taiwan 115

Edited by Lonnie O. Ingram, University of Florida, Gainesville, FL, and approved September 23, 2016 (received for review April 6, 2016)

Clostridium thermocellum **can ferment cellulosic biomass to formate and other end products, including CO_2. This organism lacks formate dehydrogenase (Fdh), which catalyzes the reduction of CO_2 to formate. However, feeding the bacterium ^{13}C-bicarbonate and cellobiose followed by NMR analysis showed the production of ^{13}C-formate in *C. thermocellum* culture, indicating the presence of an uncharacterized pathway capable of converting CO_2 to formate. Combining genomic and experimental data, we demonstrated that the conversion of CO_2 to formate serves as a CO_2 entry point into the reductive one-carbon (C1) metabolism, and internalizes CO_2 via two biochemical reactions: the reversed pyruvate:ferredoxin oxidoreductase (rPFOR), which incorporates CO_2 using acetyl-CoA as a substrate and generates pyruvate, and pyruvate-formate lyase (PFL) converting pyruvate to formate and acetyl-CoA. We analyzed the labeling patterns of proteinogenic amino acids in individual deletions of all five putative PFOR mutants and in a PFL deletion mutant. We identified two enzymes acting as rPFOR, confirmed the dual activities of rPFOR and PFL crucial for CO_2 uptake, and provided physical evidence of a distinct in vivo "rPFOR-PFL shunt" to reduce CO_2 to formate while circumventing the lack of Fdh. Such a pathway precedes CO_2 fixation via the reductive C1 metabolic pathway in *C. thermocellum*. These findings demonstrated the metabolic versatility of *C. thermocellum*, which is thought of as primarily a cellulosic heterotroph but is shown here to be endowed with the ability to fix CO_2 as well.**

Clostridium thermocellum | pyruvate:ferredoxin oxidoreducase | formate | ^{13}C-isotopic tracing | one-carbon metabolism

The gram-positive *Clostridium thermocellum* is a thermophilic and strict anaerobic bacterium. It has gained a great amount of interest due to its cellulolytic abilities. By taking advantage of an extracellular cellulase system called the cellulosome (1), *C. thermocellum* can depolymerize cellulose into soluble oligosaccharides. The latter are further transported into the cells and fermented through its glycolytic pathway to pyruvate, the precursor to an array of fermentation products (e.g., H_2, formate, lactate, acetate, ethanol, secreted amino acids) (2, 3). This capability makes *C. thermocellum* an attractive candidate for consolidated bioprocessing of lignocellulosic biomass, a process configuration that directly converts plant biomass into biofuels and chemicals without separate additions of enzymes (4). To date, there have been numerous works describing the molecular and genetic details of the cellulolytic system and fermentation pathways in *C. thermocellum* (5–9), whereas other metabolic characteristics of this species have not been adequately understood.

Currently, few details regarding inorganic carbon utilization are known for *C. thermocellum*. However, several investigators routinely add bicarbonate, a dissolved form of CO_2, into the medium to promote *C. thermocellum* growth (6, 10–12), implying its ability to use CO_2. This observation raises the questions of how CO_2 plays a role in promoting *C. thermocellum* growth (13), and whether CO_2 is incorporated into the metabolism. There is limited information on pathways relating to CO_2 uptake thus far. One proposed pathway involving CO_2 utilization in *C. thermocellum* is the malate shunt and its variant pathway (7, 14), in which CO_2 is first incorporated by phosphoenolpyruvate carboxykinase (PEPCK) to form oxaloacetate and then is released either by malic enzyme or via oxaloacetate decarboxylase complex, yielding pyruvate. However, other pathways capable of carbon fixation may also exist but remain uncharacterized.

In recent years, isotopic tracer experiments followed by mass spectrometry (MS) (15, 16) or NMR measurements (17) have emerged as powerful tools for metabolic analysis. This methodology traces the transit of isotopic atoms throughout the biochemical network and sheds light on active reactions as well as molecular fluxes in vivo. Coupled with classic genetic manipulations, this technology has been successfully applied to provide insights into novel metabolic pathways in bacteria (18), yet it has not been used to study *C. thermocellum*.

In several species of *Clostridium*, the one-carbon (C1) metabolism is initiated from CO_2 reduction to become formate via formate dehydrogenase (Fdh) (19). This pathway provides C1 units for many crucial reactions, including amino acids and purine biosynthesis. Formate serves as a precursor to the folate biosynthesis pathway that forms the "methyl" branch of the Wood–Ljungdahl pathway, yielding acetyl-CoA from CO_2 (19). However, *C. thermocellum* lacks the first key enzyme, Fdh, based on genome information. In the present study, we investigate CO_2-fixing pathway(s) in *C. thermocellum* involving C1 metabolism by using ^{13}C-tracer experiments. We

Significance

High carbon yield in the bioengineering of heterotrophic bacteria is hindered by carbon loss to CO_2 production. We provide evidence showing *Clostridium thermocellum*, a cellulose-degrading bacterium and a model consolidated bioprocessing organism, can fix CO_2 while growing predominantly on cellobiose, a cellulose-derived disaccharide. By adding ^{13}C-bicarbonate to the bacterial culture and tracking ^{13}C-labeled metabolites, we discovered active reductive one-carbon (C1) metabolism in this bacterium. We further identified critical enzymes responsible for fixing CO_2 and channeling the fixed carbon to the C1 metabolic pathway. Our findings pave the way to future engineering of this bacterium to use cellulose and CO_2 simultaneously as a means to improve microbial carbon efficiency that is constrained by theoretical limitation and to reduce CO_2 in the environment.

Author contributions: W.X., P.P.L., L.M., L.W., J.C.L., P.-C.M., and K.J.C. designed research; W.X., P.P.L., L.M., L.W., and K.J.C. performed research; W.X., P.P.L., L.M., L.W., J.C.L., P.-C.M., and K.J.C. analyzed data; and W.X., P.P.L., L.M., L.W., J.C.L., P.-C.M., and K.J.C. wrote the paper.

The authors declare no conflict of interest.

This article is a PNAS Direct Submission.

Freely available online through the PNAS open access option.

[1]To whom correspondence may be addressed. Email: katherine.chou@nrel.gov or pinching.maness@nrel.gov.

This article contains supporting information online at www.pnas.org/lookup/suppl/doi:10.1073/pnas.1605482113/-/DCSupplemental.

measure the isotopomers of fermentation products and proteinogenic amino acids using NMR and GC/MS, and uncover a route *C. thermocellum* employs to fix CO_2 when grown in a primarily heterotrophic mode supplemented with sodium bicarbonate.

Results

Effects of Bicarbonate on *C. thermocellum* Growth and Metabolism. To examine *C. thermocellum*'s ability to use inorganic carbon, we compared cell growth and metabolic product formation during cellobiose fermentation with and without bicarbonate supplementation (20 mM). To eliminate any potential buffering effect exerted by bicarbonate, fermentation was performed in batch mode with pH controlled at 7.0 throughout. Upon consumption of all cellobiose, cultures with added bicarbonate yielded ∼40% more cell biomass than in its absence (Table 1). Without accounting for the excreted amino acids that have been observed in overflow metabolism (3), this result increased the possibility that extra total carbon output (i.e., cell biomass, lactate) could emerge from incorporation of the inorganic carbon (bicarbonate) as suggested by the calculated apparent carbon efficiency (65.7% without bicarbonate and 75.5% with bicarbonate; Table 1). We also observed higher apparent carbon efficiency in bicarbonate-fed cultures in non–pH-controlled fermentation (Table S1) buffered with 50 mM 3-(*N*-morpholino)propanesulfonic acid (MOPS).

Reduction of Bicarbonate to Formate as Revealed by NMR Analysis Using ^{13}C-Tracer. To track how bicarbonate could be metabolized by the bacterium, we fed *C. thermocellum* ^{13}C-bicarbonate (20 mM) and unlabeled cellobiose (14.6 mM) and analyzed the labeled fermentation products that were excreted into the medium with ^{13}C-NMR. Data from Fig. 1*A* show 1D ^{13}C spectra of the culture-spent medium after cells were grown to late log phase. In the medium, we detected small peaks at 160.3 and 128.0 ppm (Fig. 1*A*, double asterisks), which correspond to residual bicarbonate and CO_2, respectively (Fig. 1*A*, *Top* and *Middle*), and a signature formate carbonyl peak with a chemical shift at 171.1 ppm (Fig. 1*A*, *Middle* and *Bottom*). To confirm the formation of ^{13}C-formate further, common fermentation products were also assessed for the assignment of the new peak at 171.1 ppm. Organic acids, including succinate, malate, butyrate, citrate, and isocitrate, have carbonyl carbons with chemical shifts that do not match the observed peak. One class of doubtable compounds is alpha-keto acids (i.e., pyruvate, 2-oxoglutarate), which have a carboxylic carbon linked to a keto group, appearing at around 170 ppm. To validate further, the ^{1}H decoupling was inactivated during signal acquisition. A one-bond carbon–hydrogen scalar coupling, J_{HC}, of 195-Hz splits the peak at 171.1 ppm (Fig. 1*B*) due to a hydrogen directly bound to the carbonyl carbon. Pyruvate and 2-oxoglutarate, however, do not have directly bound ^{1}H on their respective carbonyl carbons, leading to the conclusion that the new peak at 171.1 ppm is indeed derived from formate. In addition to ^{13}C-formate, two small peaks at 182.5 and 174.4 ppm (Fig. 1*A*, marked with asterisks) correspond to other fermentation products that may also be derived from ^{13}C-bicarbonate labeling but in very small amounts. Other peaks from 5 to 65 ppm likely arose from natural abundance components in the defined media and did not change in relative intensity from sample to sample.

Putative Reductive C1 Metabolism Based on Genome Annotation. The above labeling experiments provided evidence of a significant CO_2-to-formate reduction pathway that remains to be characterized. To identify genes that are putatively responsible for this conversion, we reconstructed the C1 metabolic pathway de novo, based on the genomic information of *C. thermocellum* DSM1313 strain (20). Its genome sequence suggests that *C. thermocellum* is capable of converting formate to methionine, serine, and pyruvate via the methyl branch of the Wood–Ljungdahl pathway (Fig. 2). However, it lacks Fdh, the enzyme microbes typically use to convert CO_2 to formate (Fig. 2).

Lacking the *fdh* gene, the only other gene encoding formate production found in *C. thermocellum* genome is pyruvate-formate lyase (PFL), catalyzing the conversion of pyruvate and CoA to acetyl-CoA and formate (21). We thereby hypothesize that a bypass consisting of two reactions catalyzed by pyruvate:ferredoxin oxidoreductase (PFOR) in the reversed direction and PFL may realize the CO_2-to-formate conversion. Presumably, the reversed PFOR activity fixes CO_2 by catalyzing the formation of pyruvate using CO_2 and acetyl-CoA as cosubstrates. The fixed carbon atom from CO_2 forms the carboxylic group of pyruvate, which was then split to make formate by PFL (Fig. 2), with the remaining two carbons in pyruvate making up the acetyl group in acetyl-CoA. Both *pfl* and *pfor* genes are annotated in the *C. thermocellum* genome. Genes for pyruvate formate lyase (*pflB*, *clo1313_1717*) and its activating enzyme (*pflA*, *clo1313_1716*) are adjacent to each other on the genome. Several putative genes encoding for PFOR (*clo1313_0673*, *clo1313_0020-0023*, *clo1313_0382-0385*, and *clo1313_1353-1356*) were also annotated, hence making our hypothesis genetically feasible.

^{13}C-Tracer Data Demonstrated the Reversed PFOR Activity. To investigate this hypothesized pathway, we first test if a reversed PFOR (rPFOR) activity exists in vivo. We set up a steady-state tracer experiment by feeding ^{13}C-bicarbonate (20 mM) along with unlabeled cellobiose (14.6 mM) to the cells and detecting the labeling pattern of proteinogenic amino acids by GC/MS. The isotopomer fingerprint of pyruvate can be traced by the isotopomer fingerprint of alanine, which is a direct transaminated product of pyruvate. As shown in Fig. 3*A*, M_ala_085 is a GC/MS fragment of alanine and reveals the labeling pattern of a pyruvate fragment with carbon atoms at positions 2 and 3 (Pyr2–3). For Pyr2–3, a dominant peak at m0 accounted for 95% ($n = 3$, SE ≤ 1%) of total isotopes, suggesting that the carbon atoms at positions 2 and 3 remained almost entirely unlabeled. M_ala_057 is another MS fragment of alanine, representing the isotopomer pattern of pyruvate with all carbon atoms (Pyr1–3). The detected m0 and m1 signals accounted for 55% and 43% of total isotopes, respectively, indicating that a significant portion of this MS fragment either remained fully unlabeled or had only one ^{13}C-carbon (∼43%). These results led us to conclude that the labeled carbon is predominantly at position 1 (carboxylic group) of pyruvate, which is consistent with the hypothesized rPFOR reaction to fix CO_2

Table 1. Carbon input and output in pH-controlled bioreactors (pH 7.0) with and without bicarbonate

HCO_3^-, 20 mM	Cellobiose consumed, mM	Lactate, mM	Formate, mM	Acetate, mM	Ethanol, mM	Final OD_{600}	$C_{biomass}$,* mM	Apparent carbon efficiency†
With bicarbonate	17.2 ± 0.6	10.3 ± 1.1	3.1 ± 0.6	9.1 ± 0.4	19.9 ± 0.5	1.4 ± 0.2	63.8 ± 8.8	75.5 ± 3.0%
Without bicarbonate	17.3 ± 0.3	8.3 ± 0.1	3.8 ± 1.2	11.1 ± 0.6	21.3 ± 0.4	1.0 ± 0.3	42.9 ± 12.1	65.7 ± 5.5%

*Carbon molarity in cell biomass ($C_{biomass}$) is calculated based on the *C. thermocellum* formula $C_5H_8O_2N$ and the measured OD_{600} values (OD_{600} = 1.04 g/L cell dry weight).

†Apparent carbon efficiency is defined as the ratio of produced organic carbons to consumed organic carbons following the calculation: $(C_{lactate} + C_{formate} + C_{acetate} + C_{ethanol} + C_{biomass})/C_{cellobiose}$. Data are representative biological replica (mean ± SD, $n = 2$).

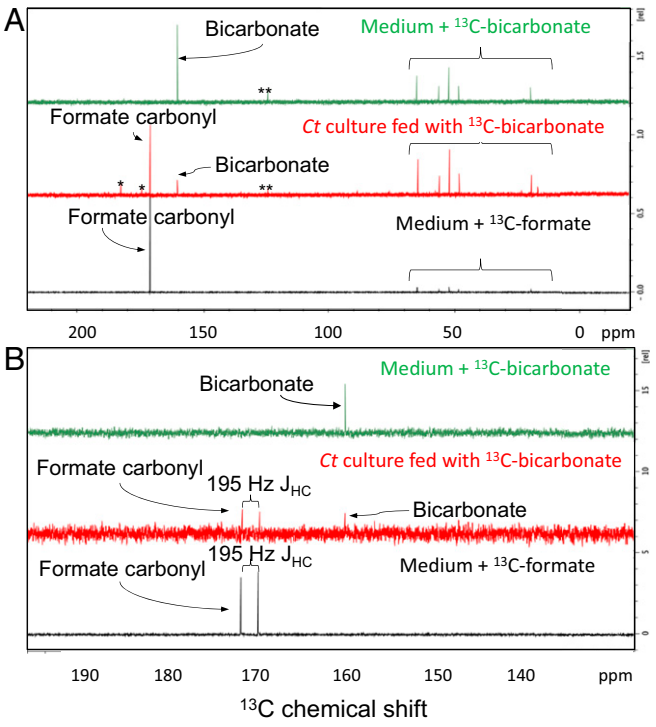

Fig. 1. ^{13}C-NMR analysis of supernatant from *C. thermocellum* (*Ct*) culture fed with 20 mM ^{13}C-bicarbonate and 14.6 mM unlabeled cellobiose. (*A*) ^{13}C-NMR signal at 171 ppm is consistent with a formate carbonyl carbon that is observed in the spent medium of *C. thermocellum* (red spectrum). Defined medium supplemented with 20 mM ^{13}C-bicarbonate (green spectrum) and 20 mM ^{13}C-formate (black spectrum) was analyzed as the references. The single asterisk indicates other products of bicarbonate metabolism. The double asterisks indicate a contaminant in the ^{13}C-bicarbonate. The signals within the braces indicate natural abundance of aliphatic and methyl carbons from the medium or metabolites. (*B*) J_{HC} dipolar coupling of 195 Hz further confirms the identification of the peak at 171 ppm as formate.

(Fig. 3*B*) and strongly supports the existence of rPFOR activity in vivo under the tested physiological condition. We also detected ^{13}C-lactate with a labeling pattern consistent with the labeling pattern of pyruvate (Figs. 2 and 3), presumably propagated from pyruvate.

To confirm rPFOR activity as the main mechanism contributing to the labeled pyruvate (position 1), and not to the label exchange reaction, we fed *C. thermocellum* [2-^{13}C]acetate (40 mM) supplemented with unlabeled bicarbonate (20 mM) when cells were grown primarily in cellobiose (5 g/L). Results showed labeled carbons at the expected position in pyruvate (position 3) and acetyl-CoA (position 2) in both wild type (Δ*hpt*; Fig. 3*C*) and PFL-inactivated mutant (Δ*hpt*Δ*pflA*; Fig. S1). For confirmation and characterization of the Δ*hpt*Δ*pflA* mutant, see Fig. 5 and Figs. S2 and S5*A*. These results also ruled out the possibility of labeled pyruvate transiting from acetyl-CoA via reversed PFL activity. Results are described in greater detail in *SI Results*. The observed labeled carbon at position 3 of pyruvate is independent of the label exchange carbon specific to the carboxyl group, unlike previously reported in *Clostridium acetobutylicum* (22).

To determine which pathway(s) may also lead to ^{13}C-labeled pyruvate at the carboxylic carbon, we examined the fate of carbon atoms among all possible candidate pathways, including the malate shunt (7, 14) which is known to assimilate and release CO_2 in *C. thermocellum*. As shown in Fig. 3*B*, CO_2 fixation is catalyzed by PEPCK, resulting in ^{13}C-labeling at position 4 of oxaloacetate. This labeled carbon is propagated to position 4 of malate via malate dehydrogenase and is subsequently lost as $^{13}CO_2$ by malic enzyme. Therefore, malate shunt, per se, does not contribute to the ^{13}C-labeling at the carboxylic group of pyruvate. Another possible carboxylase enzyme that could presumably result in the labeling at the carboxylic group of pyruvate is ribulose bisphosphate carboxylase/oxygenase (RuBisCO). However, genes encoding for the highly conserved RuBisCO enzyme are not present in the *C. thermocellum* genome or in other sequenced *Clostridium* species. Thus, RuBisCO was ruled out.

We also considered the possibility of a reversible conversion between malate and fumarate catalyzed by malate hydrolyase (Clo1313_0640). The symmetry of the fumarate molecule can interchange labeling on carbon atoms in positions 1 and 4; hence, it could contribute to the resulting ^{13}C-carboyxlic group in pyruvate. Although the alanine labeling pattern (Fig. 3*A*) cannot rule out the malate hydrolyase reaction, data from genetic KOs (Fig. 4) presented below are consistent with rPFOR activity and not malate hydrolyase activity.

We also investigated the isotopomer pattern for serine, which could be derived from phosphoglycerate, a triose phosphate interconverted with pyruvate in the glycolytic pathway (Fig. 2). Assuming that serine is exclusively derived from glycolysis and shares an identical synthetic route with alanine, the labeling pattern of serine and alanine should be very similar. However, in contrast to mostly unlabeled Pyr2–3, we observed a nonnegligible m1 peak of Ser2–3 with 12% enrichment (Fig. 3*A*). One carbon labeled at Ser2–3 implies a distinct serine pathway from pyruvate, consistent with the metabolic pathway in which a ^{13}C-methylene-THF from reductive C1 metabolism is combined with glycine by glycine hydroxymethyltransferase (*glyA*, *clo1313_1155*) and forms the hydroxylmethylene group of serine at position 3

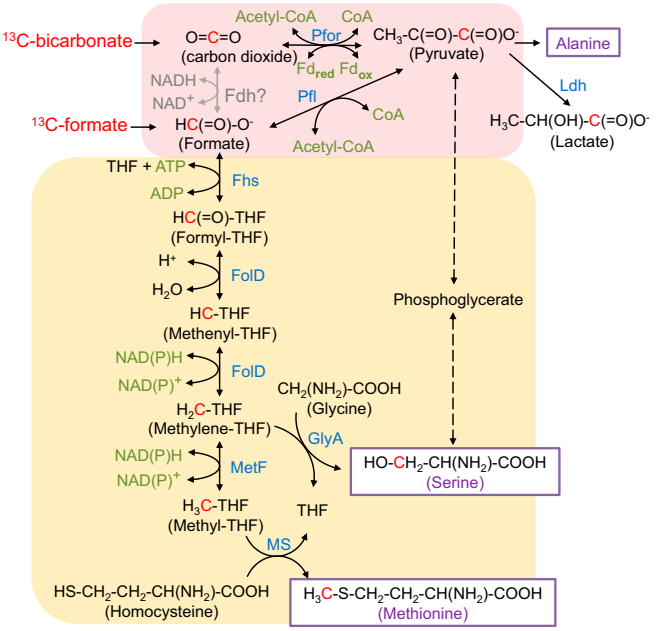

Fig. 2. Schematic of reductive C1 metabolism initiated from rPFOR and reversed PFL. The question mark indicates a missing reaction in *C. thermocellum* DSM1313 genome annotations. Pink-shaded pathways illustrate the reduction of CO_2 to formate and CO_2 to pyruvate. Yellow-shaded pathways include steps of serine and methionine biosynthesis. Fdh is not annotated in *C. thermocellum* genome. Fhs, formyl-tetrahydrofolate synthase (*clo1313_0030*); FolD, methylene-tetrahydrofolate dehydrogenase/cyclohydrolase (*clo1313_1120*); GlyA, glycine hydroxymethyltransferase (*clo1313_1155*); MetF, methylene-tetrahydrofolate reductase (*clo1313_2132*); MS, methionine synthase (*clo1313_1587-1588, clo1313_1581-1582, clo1313_0372*). Dotted lines indicate multistep catalysis. Carbons in red indicate ^{13}C-isotopes propagated from ^{13}C-bicarbonate or ^{13}C-formate in the tracer experiments.

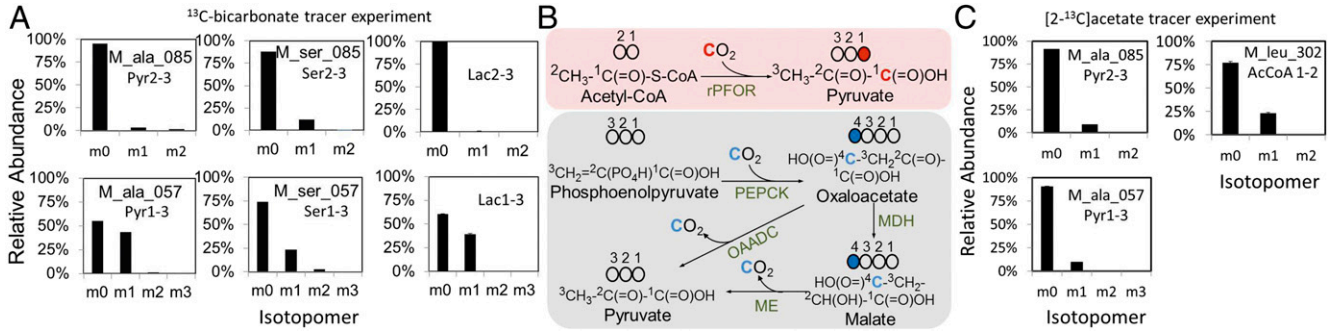

Fig. 3. Isotopomer analysis of proteinogenic amino acids and lactate in cultures grown on 20 mM ^{13}C-sodium bicarbonate and 14.6 mM unlabeled cellobiose. (*A*) Relative abundance of mass isotopomers for pyruvate, serine, and lactate (n = 3, SD < 1%) in wild type (Δ*hpt*). (*B*) Schematics of carbon atom transits via the reversed PFOR (pink box) and the malate shunt (gray box). OAADC, oxaloacetate decarboxylase complex; MDH, malate dehydrogenase; ME, malic enzyme. The labeled (^{13}C) and unlabeled (^{12}C) carbon atoms are represented by closed and open circles, respectively. (*C*) Isotopomer analysis of proteinogenic alanine and leucine in Δ*hpt* in cultures fed with [2-^{13}C]acetate and unlabeled bicarbonate (20 mM) when the bacteria were grown primarily in 14.6 mM (5 g/L) cellobiose. Carbons at positions 1 and 2 of *N*-tert-butyldimethylsilyl-*N*-methyltrifluoroacetamide–derivatized leucine can be fragmented by GC/MS and are directly derived from acetyl-CoA.

(Fig. 2). These results implied that ^{13}C isotope propagated to pyruvate was able to flow into the C1 pathway via formate, contributing to the biosynthesis of serine in *C. thermocellum*.

Knocking Out PFOR Genes Impairs Pyruvate Synthase Activity for CO_2 Fixation. The CO_2-fixing C1 pathway initiated by PFOR in the reductive direction was further examined through the deletion of putative PFOR genes and the analysis of altered labeling patterns in the KO mutants. Multiple genes or gene clusters are annotated as PFOR (*clo1313_0020-0023*, *1353-1356*, *0673*, and *0382-0385*) or indole pyruvate ferredoxin oxidoreductase (*clo1313_1615-1616*) in the *C. thermocellum* genome. These genes were respectively deleted via homologous recombination following the schemes shown in Fig. S2*A*, and validation of the genotype via colony PCR is shown in Fig. S3 and Table S2. All PCR products were further confirmed by commercial sequencing. The resulting mutants, Δ*hpt*Δ*clo1313_0020-0023*, Δ*hpt*Δ*clo1313_1353-1356*, Δ*hpt*Δ*clo1313_1615-1616*, Δ*hpt*Δ*clo1313_0673*, and Δ*hpt*Δ*clo1313_0382-0385*, were fed with 20 mM ^{13}C-bicarbonate and 14.6 mM unlabeled cellobiose for isotope tracer experiments. The relative abundance of m0 and m1 shown for Pyr1–3 (M_ala_057; Fig. 4) and for Pyr2–3 (M_ala_085; Fig. S4) indicates that the carbon is labeled predominantly on the carboxylic group in pyruvate in both wild type (Δ*hpt*) and mutants, but the relative abundance of m1 is significantly lower in mutants Δ*hpt*Δ*clo1313_0020-0023* and Δ*hpt*Δ*clo1313_1353-1356* (Fig. 4). By taking the ratio of pyruvate labeled at the carboxylic group (m1) to unlabeled ones (m0), data showed that m1/m0 ratios are not significantly different in individual PFOR deletion mutants Δ*hpt*Δ*clo1313_1615-1616* and Δ*hpt*Δ*clo1313_0673*, or exhibited little difference in mutant Δ*hpt*Δ*clo1313_0382-0385*. However, the m1/m0 ratios are significantly lower in Δ*hpt*Δ*clo1313_0020-0023* and Δ*hpt*Δ*clo1313_1353-1356*, with reduced labeling at the carboxylic group. The results identified Clo1313_0020-0023 and Clo1313_1353-1356 functioning as a pyruvate synthase, catalyzing the incorporation of CO_2 originating from ^{13}C-bicarbonate to form pyruvate. Based on the relative ratios of m1 to m0, Clo1313_0020-0023 and Clo1313_1353-1356 account for ∼50% and 30% (Fig. 4) of pyruvate synthase activity, respectively, for carbon fixation. The differential m1/m0 ratios in these mutants also suggest that rPFOR contributes to the ^{13}C-carboxylic carbon labeling in pyruvate, which cannot originate from the interconversion between malate and fumarate alone. However, potential interplay between the putative PFORs and the interconversion between malate and fumarate is beyond the scope of this study, and hence is not addressed here.

PFL KO Mutant Is Deficient in Reductive C1 Metabolism. To assess the involvement of PFL in reductive C1 metabolism, we inactivated PFL by deleting the *pflA* gene as illustrated in Fig. S2*B*, adapting a scheme developed previously (23). Deletion of the *pflA* gene was confirmed by PCR analysis (Fig. S5*A*) and commercial sequencing of the PCR products. Mutant Δ*hpt*Δ*pflA* grew slower than the wild type in defined medium, consistent with previous observations (12). We also measured the batch fermentation products when all substrates were consumed (Fig. S5*B*). As expected, although the wild type produces 2.3 mM formate, formate is no longer detected in the Δ*hpt*Δ*pflA* culture-spent medium (Fig. S5*B*), confirming complete inactivation of PFL and the fact that PFL is the only enzyme responsible for formate production from pyruvate.

To investigate how PFL deficiency affects carbon flux toward C1 metabolism, we compared the labeling pattern of isotopomers in both Δ*hpt*Δ*pflA* and wild type by feeding ^{13}C-formate (20 mM) and ^{13}C-bicarbonate (20 mM), respectively (Fig. 5). In either case, unlabeled cellobiose (14.6 mM) was added to the cell culture. We collected isotopomer data for proteinogenic amino acids that may be synthesized from this pathway, including alanine, serine, and methionine. With the addition of ^{13}C-formate, an m1 peak with 16% enrichment in Pyr1–3 was observed for wild type, whereas the corresponding m1 ratio was merely 4% in Δ*hpt*Δ*pflA*. In the isotopomer of Pyr2–3, we observed no

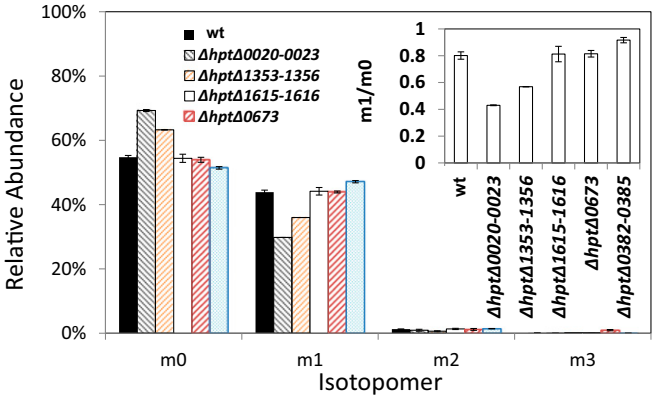

Fig. 4. Isotopomer analysis of proteinogenic alanine in Δ*hpt* and in individual deletions of all five putative PFORs. All strains were grown on 20 mM ^{13}C-sodium bicarbonate and 14.6 mM unlabeled cellobiose. (*Inset*) Ratio of m1/m0 in individual putative PFOR deletion mutants is plotted. wt, wild type.

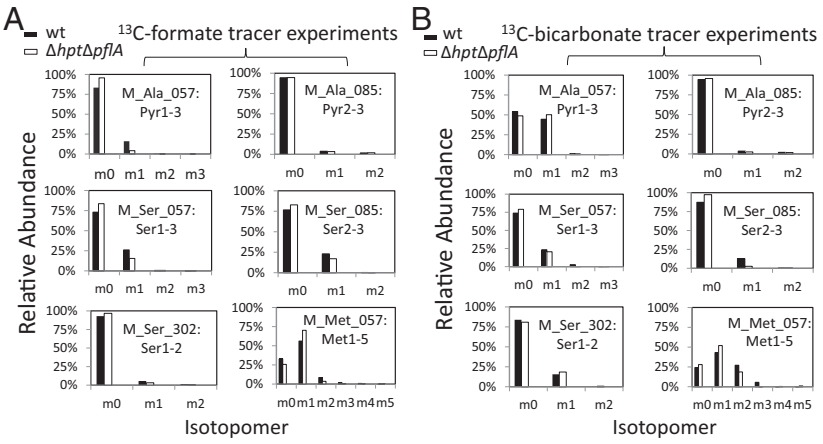

Fig. 5. Isotopomer analysis of GC/MS fragments for proteinogenic amino acids in Δ*hpt*Δ*pflA* mutant (white columns) and wild type (Δ*hpt*, black columns) grown on 14.6 mM unlabeled cellobiose with 20 mM ^{13}C-formate (*A*) or 20 mM ^{13}C-sodium bicarbonate (*B*). Panels for each GC/MS fragment represent the labeling pattern of the amino acid or its precursor with indicated C atoms. The technical variance is less than 1% in tracer experiments.

significant difference in labeling pattern between the strains. Taken together, the results supported that the ^{13}C-carbon atom in formate was internalized by the cells and became the carboxylic carbon of pyruvate, which was catalyzed by the reversed PFL activity. We next analyzed the Ser and Met isotopomers that could be synthesized from the C1 pathway downstream of ^{13}C-formate. Based on the labeling patterns of Ser1–3, Ser2–3, and Ser1–2 (Fig. 5*A*), we deduced that the ^{13}C-carbon propagated from ^{13}C-formate is mainly at position 3 of Ser (hydroxylmethylene group), consistent with our constructed de novo C1 metabolic pathway toward serine biosynthesis (Fig. 2). As for the isotopomer of Met shown in Fig. 5*A*, both Δ*hpt*Δ*pflA* and wild type indeed demonstrated a dominant peak at m1 upon ^{13}C-formate addition, validating the incorporation of the methyl group propagated from ^{13}C-formate into Met. Detailed descriptions of Ser and Met isotopomer labeling analyses are provided in *SI Results*.

We also analyzed the isotopomers of proteinogenic amino acids for ^{13}C-bicarbonate labeling experiments in Δ*hpt*Δ*pflA*. Based on our hypothesized "rPFOR-PFL shunt," incorporation of the ^{13}C-carbon from bicarbonate into the C1 metabolism is mediated by PFL, which could be validated by comparing ^{13}C-influx into the C1 metabolism in the presence and absence of an active PFL. Similar pyruvate labeling patterns were observed for wild-type and Δ*hpt*Δ*pflA* strains, both of which showed m0 and m1 dominant peaks for Pyr1–3 and m0 signal for Pyr2–3 fragment. Results suggest that *pflA* deletion does not affect CO_2 incorporation catalyzed by the pyruvate synthase activity. As for serine labeling, both Ser1–3 and Ser2–3 fragments containing the hydroxyl methylene group had a lower labeling ratio in Δ*hpt*Δ*pflA* mutant than in wild type. For Ser2–3, mutant Δ*hpt*Δ*pflA* had a much lower m1 peak (2.6%) than the control (12.7%). Correspondingly, the unlabeled m0 peak of Ser2–3 for Δ*hpt*Δ*pflA* strain is 10.1% higher than in the parental strain (97.4% vs. 87.3%). Collectively, reduced isotope enrichment in the mutant strongly supports that C1 metabolism originating from ^{13}C-bicarbonate is disrupted by knocking out *pflA*. It is also evident that PFL activity is essential in internalizing the ^{13}C-carbon in bicarbonate in *C. thermocellum*, and our hypothesis that PFL coupled with the rPFOR activity initiates the reductive C1 pathway in *C. thermocellum* was corroborated. We observed a lower extent of fractional labeling of methionine in the Δ*hpt*Δ*pflA* mutant than in wild type, which is described in greater detail in *SI Results*.

Discussion

This study reveals that during cellobiose metabolism, *C. thermocellum* also assimilates CO_2 via a reductive C1 metabolic pathway that is initiated by the dual actions of reversed PFOR and PFL. PFOR has been greatly considered in the forward direction in *C. thermocellum*, catalyzing the oxidative decarboxylation of pyruvate to acetyl-CoA and CO_2 and generating reduced ferredoxin (Fd_{red}). The PFOR activity in *C. thermocellum* has been associated with the oxidative decarboxylation of pyruvate to acetyl-CoA. Uyeda and Rabinowitz (24, 25) and Raeburn and Rabinowitz (26) demonstrated in vitro that low potential electron donors, such as Fd_{red}, can drive PFOR to catalyze the reductive carboxylation of acetyl-CoA as a pyruvate synthase. The rPFOR serves as a key enzyme for autotrophic CO_2 fixation via the Wood–Ljungdahl pathway in acetogens (27). In this work, the in vivo isotopomer data measured postfeeding *C. thermocellum* ^{13}C-biocarbonate and [2-^{13}C] acetate double-confirmed rPFOR activity and revealed that rPFOR activity accounted for over 40% of the labeled carbon in pyruvate. Measurements in individual PFOR mutants further identified rPFOR activity predominantly catalyzed by Clo1313_0020-0023 and Clo1313_1353-1356. Consistent with previous global expression studies, Clo1313_0020-0023 is the most highly expressed PFOR based on proteomics (28) and transcriptomics (29) analyses. Clo1313_1353-1356 is the third most highly expressed PFOR based on proteomics data, but it has a low transcript level based on microarray data, and the difference could be due to different growth conditions in these studies.

By feeding ^{13}C-bicarbonate to the PFL-inactivated mutant and the wild type, we confirmed the incorporation of these tracers into formate (Fig. 1), lactate (Fig. 3*A*), and the downstream amino acids linked to C1 metabolism (Figs. 3 and 5). We provided multiple lines of evidence showing that the fixed CO_2 was channeled to the C1 metabolism through PFL, which could operate reversibly (21, 30) and contribute to the biosynthesis of essential amino acids, including serine and methionine. In addition, the reductive C1 pathway mediated by PFL may play a critical role in nucleotide biosynthesis (reconstructed purine biosynthesis pathway in *C. thermocellum* shown in Fig. S6). The impaired growth observed in PFL-inactivated mutant is consistent with a previous finding (12) and underscores PFL's importance. A transcriptome study reported that folate-dependent enzymes are in the most highly expressed category, which also suggests an active C1 metabolism in vivo (31).

Carbon loss in the form of CO_2 from the conversion of pyruvate to acetyl-CoA across a wide range of bacterial heterotrophs reduces the theoretical maximum yield of a carbon product of interest per carbon consumed (carbon efficiency) downstream of acetyl-CoA. A synthetic nonoxidative glycolysis has been shown to bypass the loss of CO_2 in the conversion of pyruvate to acetyl-CoA (32). The rPFOR activity shown here allows some of the lost CO_2 to be recaptured into pyruvate, a critical branch point and precursor to numerous natural and nonnatural products. Based on our data, CO_2 utilization has increased the titers of organic carbon compounds (Table 1) by incorporating CO_2 into the biomass

formula, as detected in proteinogenic serine and methionine, and, as such, supplementing cell growth.

It is interesting that *C. thermocellum* uses the rPFOR-PFL shunt for CO_2 uptake in the absence of Fdh. We speculate that although pyruvate is a key branching point in central carbon metabolism and a key node connecting glycolysis and the C1 metabolic pathway, the rPFOR-PFL route for CO_2 uptake may provide added metabolic flexibility and versatility to cells in response to environmental changes affecting their carbon and energy (redox) needs. To gain insights into how widespread the rPFOR-PFL shunt could be for CO_2 uptake, we surveyed the presence of PFOR, PFL, and Fdh in 67 sequenced *Clostridium* species. We discovered that only 20 species have Fdh, whereas 51 species have both PFOR and PFL (Fig. S7). Although the in vivo reversibility of PFOR can be organism- and/or growth condition-specific, and information as to whether these bacteria can use inorganic carbon during organic substrate feeding may not be readily available, the presence of these genes renders it genetically feasible.

It should be noted that carbon fixation via the rPFOR-PFL shunt requires Fd_{red} as an electron donor. On the other hand, PFOR functioning in the oxidative direction serves as a major pathway for generating Fd_{red} to yield reduced biofuels and chemicals. Thus, the metabolic flux toward biosynthesis may be a trade-off of the flux toward electron generation. We speculate that CO_2 enhances growth by regenerating oxidized Fd, which, in turn, provides a driving force for faster cellobiose consumption. Feeding CO_2 may also enhance the "transient" CO_2 fixation via the malate shunt, with GTP produced via PEPCK promoting *C. thermocellum* growth. The biosynthesis vs. energy requirement at the pyruvate node needs to be evaluated comprehensively with other major redox pathways (i.e., H_2 production) to enhance the carbon economy without causing redox imbalance. To satisfy our curiosity, we tested *C. thermocellum* autotrophic growth by feeding either bicarbonate plus 100% H_2 or an 80% H_2/20% (vol/vol) CO_2 gas mixture, but detected no growth (Fig. S8). Nevertheless, the rPFOR-PFL shunt uncovered in this study may have important ramifications in the metabolic plasticity of a cellulose degrader and in other heterotrophs, and hence warrants more in-depth investigations.

Materials and Methods

A more complete discussion is provided elsewhere (15, 16, 23, 33–35), as well as in *SI Methods*.

Unless otherwise noted, *C. thermocellum* DSM1313-derived strains, Δ*hpt* (*hpt* encoding for hypoxanthine phosphoribosyl transferase is used for counterselection), and other mutants were routinely grown anaerobically at 55 °C on 5 g/L cellobiose. The *hpt* gene deleted strain is used as the wild type for the studies herein. To test the inorganic carbon utilization, 20 mM sodium bicarbonate was added to cell cultures also fed with cellobiose. We used the DSM122-defined medium referred to as CTFUD medium (36). Full details on strain construction, fermentation conditions, and ^{13}C-tracer experiments are provided in *SI Methods*.

ACKNOWLEDGMENTS. We thank Chris Urban, Maria Chun, Sawako Konishi, and Sharon C. Xu for their technical assistance. This work was supported by the National Renewable Energy Laboratory (NREL) Director's Fellowship (Laboratory Directed Research and Development Subtask 06271403) (to W.X.), and the US Department of Energy (DOE) Energy Efficiency and Renewable Energy (EERE) Fuel Cell Technologies Office (K.J.C., L.M., and P.-C.M.) under Contract DE-AC36-08-GO28308. L.W. and research conducted at the University of California, Los Angeles (P.P.L. and J.C.L.) were supported by the BioEnergy Science Center (BESC), a US DOE Bioenergy Research Center supported by the Office of Biological and Environmental Research in the DOE Office of Science.

1. Gold ND, Martin VJ (2007) Global view of the *Clostridium thermocellum* cellulosome revealed by quantitative proteomic analysis. *J Bacteriol* 189(19):6787–6795.
2. Ellis LD, et al. (2012) Closing the carbon balance for fermentation by *Clostridium thermocellum* (ATCC 27405). *Bioresour Technol* 103(1):293–299.
3. Holwerda EK, et al. (2014) The exometabolome of *Clostridium thermocellum* reveals overflow metabolism at high cellulose loading. *Biotechnol Biofuels* 7(1):155.
4. Olson DG, McBride JE, Shaw AJ, Lynd LR (2012) Recent progress in consolidated bioprocessing. *Curr Opin Biotechnol* 23(3):396–405.
5. Nataf Y, et al. (2010) *Clostridium thermocellum* cellulosomal genes are regulated by extracytoplasmic polysaccharides via alternative sigma factors. *Proc Natl Acad Sci USA* 107(43):18646–18651.
6. Zhou J, et al. (2013) Atypical glycolysis in *Clostridium thermocellum*. *Appl Environ Microbiol* 79(9):3000–3008.
7. Deng Y, et al. (2013) Redirecting carbon flux through exogenous pyruvate kinase to achieve high ethanol yields in *Clostridium thermocellum*. *Metab Eng* 15:151–158.
8. Zhang YH, Lynd LR (2005) Cellulose utilization by *Clostridium thermocellum*: Bioenergetics and hydrolysis product assimilation. *Proc Natl Acad Sci USA* 102(20):7321–7325.
9. Lu Y, Zhang YH, Lynd LR (2006) Enzyme-microbe synergy during cellulose hydrolysis by *Clostridium thermocellum*. *Proc Natl Acad Sci USA* 103(44):16165–16169.
10. Lin PP, et al. (2015) Consolidated bioprocessing of cellulose to isobutanol using *Clostridium thermocellum*. *Metab Eng* 31:44–52.
11. Lo J, Zheng T, Hon S, Olson DG, Lynd LR (2015) The bifunctional alcohol and aldehyde dehydrogenase gene, adhE, is necessary for ethanol production in *Clostridium thermocellum* and *Thermoanaerobacterium saccharolyticum*. *J Bacteriol* 197(8):1386–1393.
12. Rydzak T, Lynd LR, Guss AM (2015) Elimination of formate production in *Clostridium thermocellum*. *J Ind Microbiol Biotechnol* 42(9):1263–1272.
13. Zertuche L, Zall RR (1982) A study of producing ethanol from cellulose using *Clostridium thermocellum*. *Biotechnol Bioeng* 24(1):57–68.
14. Taillefer M, Rydzak T, Levin DB, Oresnik IJ, Sparling R (2015) Reassessment of the transhydrogenase/malate shunt pathway in *Clostridium thermocellum* ATCC 27405 through kinetic characterization of malic enzyme and malate dehydrogenase. *Appl Environ Microbiol* 81(7):2423–2432.
15. Xiong W, Liu L, Wu C, Yang C, Wu Q (2010) ^{13}C-tracer and gas chromatography-mass spectrometry analyses reveal metabolic flux distribution in the oleaginous microalga *Chlorella protothecoides*. *Plant Physiol* 154(2):1001–1011.
16. Nanchen A, Fuhrer T, Sauer U (2007) Determination of metabolic flux ratios from ^{13}C-experiments and gas chromatography-mass spectrometry data: Protocol and principles. *Methods Mol Biol* 358:177–197.
17. Szyperski T, et al. (1999) Bioreaction network topology and metabolic flux ratio analysis by biosynthetic fractional ^{13}C labeling and two-dimensional NMR spectroscopy. *Metab Eng* 1(3):189–197.
18. Xiong W, et al. (2015) Phosphoketolase pathway contributes to carbon metabolism of cyanobacteria. *Nat Plants* 2:15187.
19. Schuchmann K, Müller V (2014) Autotrophy at the thermodynamic limit of life: A model for energy conservation in acetogenic bacteria. *Nat Rev Microbiol* 12(12):809–821.
20. Feinberg L, et al. (2011) Complete genome sequence of the cellulolytic thermophile *Clostridium thermocellum* DSM1313. *J Bacteriol* 193(11):2906–2907.
21. Thauer RK, Kirchniawy FH, Jungermann KA (1972) Properties and function of the pyruvate-formate-lyase reaction in clostridiae. *Eur J Biochem* 27(2):282–290.
22. Amador-Noguez D, et al. (2010) Systems-level metabolic flux profiling elucidates a complete, bifurcated tricarboxylic acid cycle in *Clostridium acetobutylicum*. *J Bacteriol* 192(17):4452–4461.
23. Argyros DA, et al. (2011) High ethanol titers from cellulose by using metabolically engineered thermophilic, anaerobic microbes. *Appl Environ Microbiol* 77(23):8288–8294.
24. Uyeda K, Rabinowitz JC (1971) Pyruvate-ferredoxin oxidoreductase. IV. Studies on the reaction mechanism. *J Biol Chem* 246(10):3120–3125.
25. Uyeda K, Rabinowitz JC (1971) Pyruvate-ferredoxin oxidoreductase. 3. Purification and properties of the enzyme. *J Biol Chem* 246(10):3111–3119.
26. Raeburn S, Rabinowitz JC (1971) Pyruvate: Ferredoxin oxidoreductase. II. Characteristics of the forward and reverse reactions and properties of the enzyme. *Arch Biochem Biophys* 146(1):21–33.
27. Furdui C, Ragsdale SW (2000) The role of pyruvate ferredoxin oxidoreductase in pyruvate synthesis during autotrophic growth by the Wood-Ljungdahl pathway. *J Biol Chem* 275(37):28494–28499.
28. Rydzak T, et al. (2012) Proteomic analysis of *Clostridium thermocellum* core metabolism: Relative protein expression profiles and growth phase-dependent changes in protein expression. *BMC Microbiol* 12:214.
29. Raman B, McKeown CK, Rodriguez M, Jr, Brown SD, Mielenz JR (2011) Transcriptomic analysis of *Clostridium thermocellum* ATCC 27405 cellulose fermentation. *BMC Microbiol* 11:134.
30. Zelcbuch L, et al. (2016) Pyruvate formate-lyase enables efficient growth of *Escherichia coli* on acetate and formate. *Biochemistry* 55(17):2423–2426.
31. Riederer A, et al. (2011) Global gene expression patterns in *Clostridium thermocellum* as determined by microarray analysis of chemostat cultures on cellulose or cellobiose. *Appl Environ Microbiol* 77(4):1243–1253.
32. Bogorad IW, Lin TS, Liao JC (2013) Synthetic non-oxidative glycolysis enables complete carbon conservation. *Nature* 502(7473):693–697.
33. Kruger NJ, Masakapalli SK, Ratcliffe RG (2014) Optimization of steady-state ^{13}C-labeling experiments for metabolic flux analysis. *Methods Mol Biol* 1090:53–72.
34. Delaglio F, et al. (1995) NMRPipe: A multidimensional spectral processing system based on UNIX pipes. *J Biomol NMR* 6(3):277–293.
35. Helmus JJ, Jaroniec CP (2013) Nmrglue: An open source Python package for the analysis of multidimensional NMR data. *J Biomol NMR* 55(4):355–367.
36. Olson DG, Lynd LR (2012) Transformation of *Clostridium thermocellum* by electroporation. *Methods Enzymol* 510:317–330.

MICROBIOLOGY